Ge_{136} type-II clathrate as precursor for the synthesis of metastable germanium polymorphs: A computational study

Daniele Selli,[1] Igor A. Baburin,[2] Roman Martoňák,[3] and Stefano Leoni[1]
[1]*Cardiff University, School of Chemistry, Park Place, CF10 3AT Cardiff, United Kingdom*
[2]*Technische Universität Dresden, Institut für Physikalische Chemie, 01062 Dresden, Germany*
[3]*Department of Experimental Physics, Comenius University, Mlynská Dolina F2, 842 48 Bratislava, Slovakia*

(Received 12 August 2022; accepted 25 October 2022; published 8 November 2022)

The response to compression of the clathrate type-II structure Ge(cF136) is investigated by means of *ab initio* small-cell metadynamics at different temperatures and pressures. Amorphous intermediates obtained from the collapse of Ge_{136} rapidly crystallize into different end products, depending on the choice of thermodynamic parameters. At lower pressure $p = 2.5$ GPa the metastable metallic bct-5 phase competes against β-Sn [Ge(tI4)], which forms at higher pressures. Upon lowering the temperature, amorphous intermediates are instrumental to the formation of denser structural motifs, from which metallic bct-5 can form. Therein, anisotropic box fluctuations promote phase formation. The metadynamics runs are analyzed in depth using a set of topological descriptors, including coordination sequence and ring statistics. Differences in the structural landscape history and amorphous intermediates are critical for the selective formation of particular metastable polymorphs. Their understanding opens possibilities towards turning crystal structure predictions into actual materials, via identifying viable kinetic routes.

DOI: 10.1103/PhysRevB.106.174102

I. INTRODUCTION

Group-IVa elements (tetrels) display an extended polymorphism, reflected in a wide range of properties. Due to their technological relevance, semiconducting silicon and germanium have motivated repeated investigations on their polymorphism [1–6]. Germanium displays higher carrier mobility than silicon and finer band-gap tunability [7]. In Ge, lowering of phonon frequencies promotes electron-phonon coupling towards superconductivity [2,3]. Metallization occurs in silicon and germanium upon compression [1]. The possibility of metallic germanium under room conditions is very intriguing and intensively debated [2,8,9], while pressure favors superconductivity in elemental Ge [3].

The polymorphism of germanium echoes in many respects that of silicon [1] by comparatively higher transition pressures [10]. Upon compression, semiconducting Ge(cF8) transforms into the β-tin type (tI4, space group $I4_1/amd$) at about 10 GPa [11], followed by an $Imma$ phase [12], a simple hexagonal phase ($P6/mmm$) [13], an orthorhombic $Cmca$ phase [14], and finally, upon further compression above 180 GPa, the hexagonal close-packed arrangement ($P6_3/mmc$) [14]. Additional metastable polymorphs can be expected, if high-pressure experiments are designed to influence nucleation, by changed decompression protocols, by low temperatures [15], by nonhydrostaticity [16,17], or by choosing a different Ge allotrope as the starting material [18].

Open-framework structures such as clathrates [19–21] offer manifold opportunities to tune their electronic, magnetic, spectral, and transport properties, including thermoelectricity [22–26]; therefore this class of compounds is enjoying renewed interest. The type-II clathrate Ge(cF136) was chemically synthesized from a salt precursor, $Na_{12}Ge_{17}$, by mild oxidation with HCl. It is stable under room conditions and persists up to 693 K [27]. Other reported metastable modifications, Ge(tP12) and Ge(cI16) (γ-silicon type, BC8), can be generated by decompression [28–30], while Ge(hR8) [17] results from direct compression of cF136. In all these allotropes, the four-bonded atoms adopt nearest-neighbor distances that are similar to those of diamond-type Ge(cF8).

In order to systematically approach the study of phase-transition mechanisms, the use of molecular dynamics accelerated techniques is mandatory to efficiently overcome high energy barriers. Metadynamics [31] explores free-energy surfaces by depositing a history-dependent bias along selected collective variables (CVs). To investigate pressure-induced polymorphism, the whole cell can act as a CV [32–34]. In a previous work [35], we have used metadynamics to investigate structural transformations between diamond Ge(cF8) and Ge(tI4), β-Sn-type structure. Along the diamond $\rightarrow$ β-tin transition, the metadynamics visited an intermediate of bct-5 topology ($I4/mmm$).

This hypothetical structure, in which Ge atoms are five-fold coordinated, is metallic, mechanically stable under room conditions, and superconducting at room temperature. In the metadynamics run, only one box parameter was markedly affected, suggesting nonhydrostatic shearing as the protocol of choice when attempting to obtain bct-5.

Despite the noticeable differences in atomic volumes (24.5 and 28.3 Å^3, respectively), the compressibility of Ge(cF136), as revealed by the bulk moduli $B_0 = 76 \pm 6$ GPa [17], is very close to the value of cubic diamond Ge(cF8), $B_0 = 75$ GPa

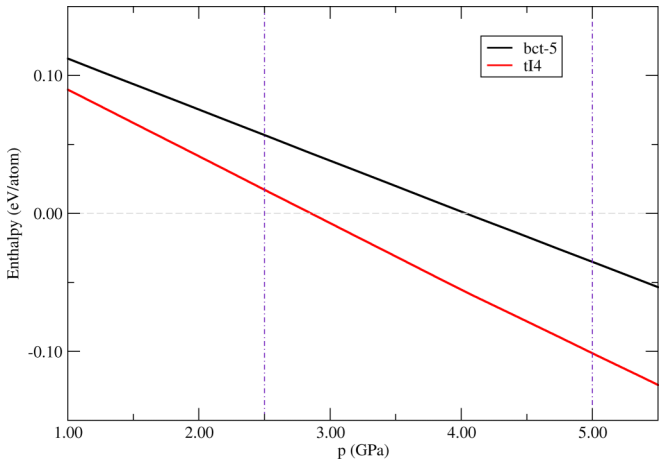

FIG. 1. Enthalpy differences between Ge_{136} [Ge(cF136)], β-tin [Ge(tI4)], and bct-5. Ge_{136} represents the baseline. The pressure values considered in this paper are indicated as vertical lines at 2.5 and 5.0 GPa.

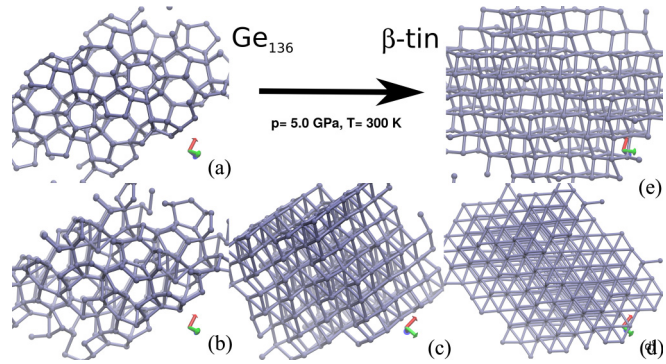

FIG. 2. (a)–(e) Snapshots from a metadynamics trajectory at $p = 5.0$ GPa and $T = 300$ K. The corresponding time steps are indicated in Fig. 3 as thick marks on the horizontal axis. Ge_{136} (a) transforms into β-tin [Ge(tI4)] (e). The metatrajectory visits a number of intermediates [(b)–(d)] as shown; refer to text for details.

[36]. Total energy calculations (using the density functional method SIESTA [37]) indicate that Ge(cF136) is the energetically lowest-lying modification among metastable germanium polymorphs.

The transition pressures between cF136, cI4, and bct-5 were evaluated based on the enthalpy equivalence between phases, $E_1 + pV_1 = E_2 + pV_2$. The difficulty in accessing bct-5 from direct, isotropic compression lies in the presence and higher relative stability of β-tin. A strategy must therefore be designed that takes into account nonhydrostatic compression (see above and Ref. [35]) of a suitable intermediate as learned from a recent study [38]. In the latter, the pressure-induced amorphization of Ge_{136} and subsequent fast recrystallization into β-tin or transformation into low-density amorphous (LDA) Ge were investigated using *ab initio* molecular dynamics and metadynamics. Metadynamics was used up to the occurrence of amorphous intermediates in the 136-atom box, followed by plain equilibrium molecular dynamics protocols until phase crystallization. Fast recrystallization was also observed in very high density amorphous (VHDA) Si [39] recently, likely owing to common tetrahedral structural motifs.

In this paper, differently from Ref. [38], we apply metadynamics beyond the stage of system amorphization to systematically identify configurations kinetically accessible from disordered intermediates. Two simulation pressures were therefore selected, $p = 5.0$ GPa and $p = 2.5$ GPa, above and below the threshold pressure for β-tin [Ge(tI4); Fig. 1]. All small-cell metadynamics runs were performed based on the 34-atom primitive cell of Ge_{136}. The choice of a small simulation box shall favor anisotropic box fluctuations and also assist disordered-ordered system transitions as demonstrated by small-cell molecular dynamics applied to ice polymorphism [40].

II. RESULTS

In Fig. 2, five metatrajectory snapshots from type-II clathrate Ge(cF136) to Ge(tI4) at $p = 5.0$ GPa and $T = 300$ K are shown, while Fig. 3 summarizes the evaluated descriptors for the same metatrajectory. The percentage of pure β-tin species is displayed on the opposite y axis in Fig. 3 (indigo curve). The metasteps corresponding to the snapshots of Fig. 2 are indicated in Fig. 3 as thick marks on the horizontal axis and labeled (Ge_{136}, I1, I2, I3, and β-tin).

The stability of Ge(cF136) is reflected in the large number of metasteps spent lingering in the initial basin. Only after more than 100 ps (about 210 metasteps) a sudden enthalpy drop (Fig. 3, main panel) is observed, as the system moves into a regime of amorphous but rather dense structures [Fig. 2(b) and intermediate I1 in Fig. 3]. The average circuit size (ACS) [41] and enthalpy display, in fact, minima, while the coordination sequence (CS; Fig. 3, right inset), which is a set of integers $\{n_1, n_2, \ldots\}$, where n_i indicate the number of atoms separated from a central one by a minimal path of i bonds, rapidly increases. Subsequently, the system remains of mixed

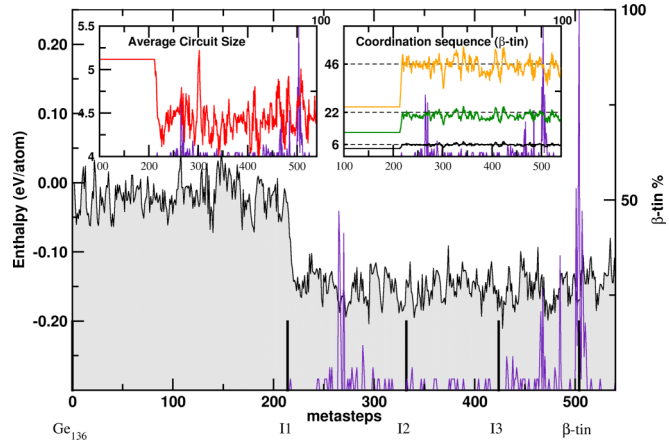

FIG. 3. Evolution of structure descriptors for the metadynamics trajectory of Fig. 2: Average circuit size (left inset), coordination sequence (right inset), and enthalpy per atom (main panel). Completion of the transformation of Ge_{136} into β-tin is represented as an indigo curve. Thick marks on the horizontal axis of the main panel correspond to the metasteps of the five snapshots represented in Figs. 2(a)–2(e).

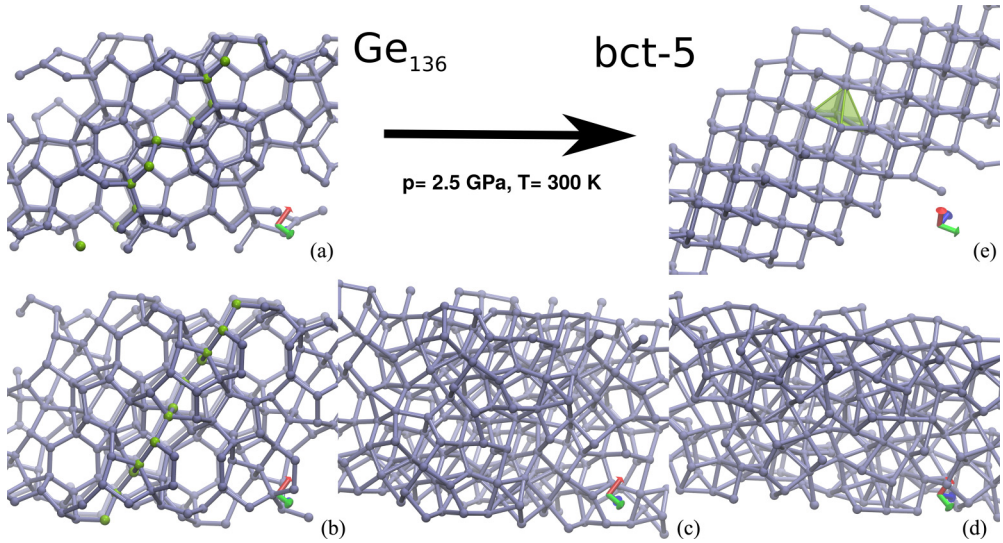

FIG. 4. (a)–(e) Snapshots from a metadynamics trajectory at $p = 2.5$ GPa and $T = 300$ K. The corresponding time steps are indicated in Fig. 5 as thick marks on the horizontal axis. Ge_{136} (a) transforms into bct-5 (e). An unstable clathrate structure Ge(mC68) is visited (b). In (a) and (b), selected Ge atoms are highlighted in green to stress the closeness between the two structural motifs. The characteristic square-pyramidal coordination polyhedron of bct-5 is shaded in green in (e).

structural character, as measured by the above indicators, with a single attempt at forming β-tin (indigo peaks) around metastep 265.

The ACS peak between metasteps 295 and 305 corresponds to a marked drop in the coordination sequence. In this region, thermal fluctuations bring the system close to β-tin (Fig. 3, β-tin %); however, the structure remains rather expanded and does not fully lock in. The configuration at metastep 332 [Fig. 2(c) and intermediate I2 in Fig. 3] is representative for the subsequent 40 metasteps and contains mixed structural motifs, comprising remaining β-tin-like features (4+2 coordination) and higher coordination numbers up to 12.

Between metasteps 370 and 400, plateaus can be recognized by inspection of the ACS, CS, and enthalpy graphs. This region features structures that are related to α-polonium type (cP1) but distorted (while Ge is on average sixfold coordinated, the angles of the octahedral coordination polyhedron deviate from 90°) and more dense, as displayed by the coordination sequence average 6, 18, 42 against the expected 6, 18, 38 for ideal α-polonium (cP1). A similar occurrence of a denser structural motif is observed between steps 405 and 425, where a simple hexagonal structural pattern is closely matched [Fig. 2(d) and intermediate I3 in Fig. 3], with a slightly expanded volume though, as can be inferred from the coordination sequence 7.5, 25, 54 against 8, 26, 56 of ideal hP1. Cell fluctuation enhancements are characteristic of the metadynamics methods and contribute to driving the systems to the final β-tin basin, into which the whole system has transformed [Fig. 3, β-tin %, and Fig. 2(e)] after about 500 metasteps.

The same descriptors were applied to a metatrajectory at $p = 2.5$ GPa and $T = 300$ K that connects Ge(cF136) to bct-5 (Figs. 4 and 5). The percentage of pure bct-5 appears on the opposite y axis in Fig. 5 (blue curve). The lower-pressure regime markedly affects the metatrajectory. After about 175 metasteps, Ge(cF136) distorts into an intermediate, which can be quenched [Fig. 4(b) and intermediate I1 in Fig. 5].

We characterized this intermediate with the Pearson symbol Ge(mC68). This clathratelike structure is higher in energy than Ge(cF136) [$\Delta E = E(\text{cF8}) - E(\text{cF136}) = 0.03$ eV/atom, while $\Delta E = E(\text{cF8}) - E(\text{mC68}) = 0.16$ eV/atom] and can be relaxed in all parameters at 0 K. The chosen projection of Figs. 4(a) and 4(b) allows us to appreciate the structural closeness of Ge(cF136) and Ge(mC68). A set of atoms has been highlighted [green spheres in Figs. 4(a) and 4(b)] to illustrate the formation of chains as part of the transforma-

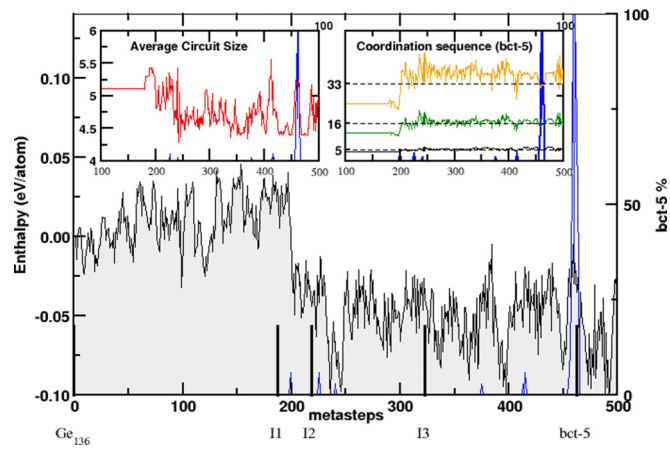

FIG. 5. Evolution of structure descriptors for the metadynamics trajectory of Fig. 4: Average circuit size (left inset), coordination sequence (right inset), and enthalpy per atom (main panel). Completion of the transformation of Ge_{136} into bct-5 is represented as a blue curve. Thick marks on the horizontal axis of the main panel correspond to the metasteps of the five snapshots represented in Figs. 4(a)–4(e).

tion mechanism, which leaves large portions of Ge(cF136) unaffected. A short molecular dynamics run started from Ge(mC68) ($t = 10$ ps, $p = 0$ GPa, $T = 300$ K) did not show any appreciable structural deformation. Nonetheless, imaginary frequencies were found in the phonon dispersion analysis (not shown), suggesting overall mechanical instability. In fact, after 25 metasteps, mC68 evolves into another structural area. Here a single structural motif can hardly be extracted, for what can be described as intermediate configurations between Ge(cF136) and a denser, β-tin-like phase: The average circuit size for this segment is ∼4.9, intermediate between 5.1 for Ge(cF136) and 4.67 for β-tin; the coordination sequence has also increased with respect to Ge(cF136), indicating overall denser structures [Fig. 4(c) and intermediate I2 in Fig. 5], while the enthalpy also takes intermediate values.

Thereafter, a long segment of the trajectory of about 175 metasteps consists of amorphous structures that occasionally show local order in correspondence to maxima in ACS and in CS, and to enthalpy minima. A representative snapshot is displayed in Fig. 4(d) (Fig. 5, intermediate I3).

At metastep 430 the metadynamics trajectory reaches the basin of bct-5, as indicated by blue peaks in Fig. 5. Its characteristic fivefold coordination is illustrated by a green pyramidal polyhedron in Fig. 4(e). bct-5 appears in a region of higher enthalpy values, corresponding to a tiny local minimum. The bct-5 motif forms within a landscape dominated by low-crystalline motifs, from which β-tin crystallization is not observed.

Two relevant pressure protocols can therefore be identified. At relatively low pressure ($P = 2.5$ GPa), a transition from Ge_{136} to bct-5 can be observed, proceeding over amorphous intermediate steps. While higher pressure always favors the formation of Ge(tI4) from Ge(cF136), lower pressures admit bct-5 among the accessible configurations. Nonetheless, even in a pressure regime below its stability range such as the one implemented here, Ge(tI4) remains a common transient motif linking fourfold to higher coordinations. This shows the need for a thorough investigation of the factors that may determine the appearance of bct-5.

The metadynamics from Ge(cF136) was repeated at 5.0 GPa and 77 K, using the same protocol as for the previous runs. Lowering temperature caused the β-tin phase to sharply lock in, with a clear signature on the enthalpy profile, and this phase remained well defined over many metasteps, as shown in Fig. 6. Also, the transition was markedly smoother as indicated by the gentle drop in the enthalpy profile, the overall progressive drop in the ACS, and the increase in the CS.

As the system escapes the Ge(cF136) well, it visits an open-framework structure (metasteps 300–310) which is denser than the initial structure and which displays a minimum in the ACS and an increased CS value (Fig. 6, left and right insets). This is less of a metastable phase than an activated intermediate, which is followed by a region of amorphous structures, as any coherent structural motif is hardly distinguishable, while neither ACS nor CS indicate the existence of a clearly defined intermediate crystalline structure.

Around metastep 380 the system recrystallizes into a β-tin-like structure (maximum in ACS and minima in CS values and enthalpy). Cell fluctuations bring it back to an amorphous

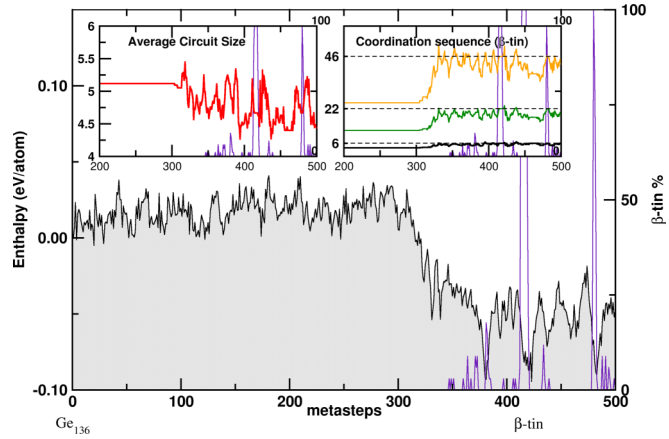

FIG. 6. Evolution of structure descriptors for a metadynamics trajectory ($p = 5.0$ GPa, $T = 77$ K): Average circuit size (left inset), coordination sequence (right inset), and enthalpy per atom (main panel). Completion of the transformation of Ge_{136} into β-tin is represented as an indigo curve.

stage, which is the gateway to the exact β-tin basin. Between two 100% β-tin peaks centered at metasteps 416 and 480, other amorphous phases are touched upon. Nonetheless, it can be expected that these effects can be further affected by retuning the choice of the Gaussian parameters in the simulation setup.

The metadynamics run at $p = 2.5$ GPa and $T = 77$ K was performed with a slightly modified protocol, which entailed rescaling the width and height of the Gaussian bias (see Sec. V for details). The rescaling to a lower value would, namely, allow for a longer persistence in stable basins. A full analysis based on the same descriptors as for the other runs (enthalpy, ACS, and CS), augmented by the statistics of fivefold rings (green curve), is presented in Fig. 7, main panel. Fivefold rings introduce an additional means to sharply distinguish between Ge(cF136), Ge(tI4), and bct-5. Their characteristic number of fivefold rings is 180 and 136, respectively (orange labels on the opposite y axis in the main panel of Fig. 7), while there are no fivefold rings in bct-5.

In Ge(cF136) fivefold rings occur as so-called K_5 graphs [42], in which six fivefold rings share each two edges around a Ge atom. They constitute therefore characteristic building blocks based on fivefold-ring statistics, whose monitoring is therefore an excellent indicator of structure evolution.

Considering major changes only, three regions can roughly be distinguished by enthalpy in Fig. 7: A first segment from metastep 1 to metastep 660, dominated by Ge(cF136), a second region between metasteps 660 and 1330, and a third region (metasteps 1580–3260) of overall lower enthalpy (including fluctuations). The CS indicates that the first two regions are dominated by tetrahedral motifs (first CS = 4, Fig. 7, right inset, black curve), while denser structures are found in the third region. Therein, the number of fivefold rings remains largely within (occasionally above) a well-defined region (orange dashed lines in Fig. 7, main panel), while depletion of that figure occurs only episodically. In Fig. 8, eight snapshots from the metatrajectory are presented. Their corresponding metasteps are indicated on the main horizontal

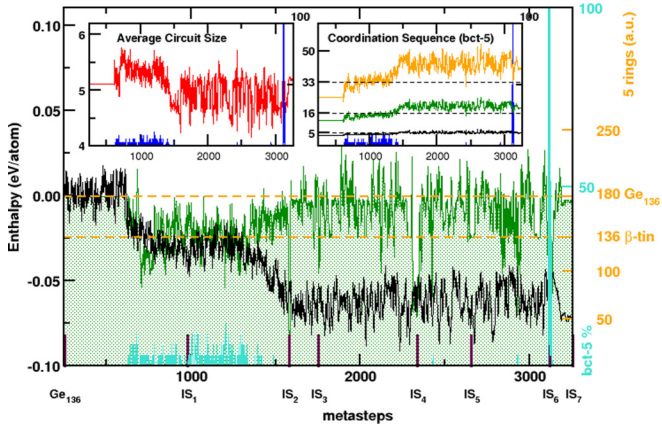

FIG. 7. Evolution of average circuit size (left inset), coordination sequence (right inset), enthalpy per atom (black curve, main panel), and number of fivefold rings (green curve, main panel), for a metadynamics run at $p = 2.5$ GPa and $T = 77$ K. Eight thick marks on the horizontal axis of the main panel indicate the metasteps relative to the eight snapshots of Figs. 8(a)–8(h). On the opposite y axis in the main panel, the characteristic number of fivefold rings for Ge_{136} and β-tin is indicated: 180 and 136, respectively (orange labels and dashed orange lines). In bct-5, there are no fivefold rings. The progress of the conversion from Ge_{136} to bct-5 is indicated as a blue (turquoise) curve in the insets (main panel).

axis in Fig. 7 (thick marks labeled Ge_{136} and IS_1–IS_7), typically corresponding to a lowering of the number of fivefold rings (green curve in Fig. 7, main panel).

Ge_{136} lasts till metastep 660 [Fig. 8(a)]. A representative configuration of the second region would still contain fivefold rings, which at this stage may be partially fused fivefold rings [Fig. 8(b) and intermediate IS_1 in Fig. 7]. After metastep 1330, structural motifs of higher fivefold-ring number are more prone to configuration fluctuations, i.e., they are rapidly evolving and do not leave any durable trace on any of the descriptors of interest, CS and enthalpy for instance. Correspondingly, configurations with fewer fivefold rings are better characterized. At metastep 2430 a spike-shaped depletion in the fivefold-ring curve corresponds to a structure which displays features of bct-5 [Fig. 8(c), square pyramid, and intermediate IS_2 in Fig. 7], which nonetheless fails to fully lock in.

This is followed by IS_3, containing a distorted, trigonal bipyramidal motif as the coordination polyhedron, and by IS_4 [Fig. 8(e)], in which a sixth atom has entered the coordination sphere. IS_5 corresponds to β-tin [metastep 2660, Fig. 8(f)] and occurs at a few other metasteps, distinguishable by the characteristic fivefold-ring number of 136 (green curve in Fig. 7, main panel). However, the signature on enthalpy is never exactly repeated and remains narrow (black curve in Fig. 7, main panel, metasteps 1820, 2028, 2660, and 3040). While thermodynamics is not favorable to the formation of IS_5 in this regime, its motif is nonetheless part of the landscape, in which it occurs as an intermediate towards other structures, including bct-5, a fact that was already noticed at higher temperature (see discussion above).

At metastep 3120, bct-5 locks in, corresponding to full fivefold-ring depletion and to a plateau of 35 metasteps in the enthalpy [Fig. 8(g); its characteristic pyramidal coordination polyhedron is shadowed in green]. Shortly thereafter (metastep 3180), bct-5 transforms into a denser (CS 5, 19, 40.5) motif, containing topologically different Ge atoms, but all fivefold coordinated. Similar to what was observed above and in a previous work [35], bct-5 is associated with local minima in a region of relatively higher enthalpy.

III. DISCUSSION

The modified metadynamics protocol with variable Gaussian shape rescaling, which results in a longer trajectory, allows for many intermediate configurations, some of which are elusive as they result from box shape fluctuations and depend therefore on the specific metadynamics bias history. The formation of Ge(tI4), β-tin, succeeded over a direct route for both temperature choices, with normally a sharp lowering of the enthalpy value, a lowering of the ACS, and a persistence of the system in denser configurations, as indicated by the CS (Figs. 3 and 6). Configurationally, Ge_{136} is rigid and requires an extended incubation time for it to transform. This is directly related to the mentioned K_5 graphs, which characterize its topology. At higher pressure (Fig. 2), removal of K_5 graphs yields shorter ACS and leads to rapid densification. At lower pressures, in contrast, intermediates (Fig. 4) appear, and many amorphous configurations.

At lower temperature and pressure, an intermediate enthalpy regime (Fig. 7) exists, without dominant motifs, but as a landscape of configurations rich in fivefold rings. By inspection of the CS and ACS, this region is substantially homogeneous and glasslike. Therein, fivefold rings can occur in different distributions, fused or separated, and are intrinsically flexible, i.e., their configuration can vary. The occurrence of fivefold rings can therefore be used to measure the distance of a given structural motif from a certain reference structure with fewer internal degrees of freedom. The contribution to combinatorial and configurational entropy of fivefold rings has been used, for example, to formulate an entropy descriptor of amorphous silicon [43,44]. The enthalpy values are lower on average as the number of fivefold rings increases (notice that enthalpy and fivefold-ring graphs are arbitrarily aligned in Fig. 7). As well, counting fivefold rings provides a stable descriptor to monitor the structural evolution within a rather disordered or amorphous regime.

The occurrence of particular structural motifs can be the result of how Gaussians are accumulated in a metadynamics run; therefore directly interpreting structural sequences into mechanisms can be flawed. Here we focus just on the last segment of the low-pressure, low-temperature metatrajectory (Figs. 7 and 8; metasteps 3120–3300). Therein, bct-5 rapidly converted into a different five-membered connected network (see above), accompanied by enthalpy lowering as the fivefold-ring numbers increased. The square pyramid around Ge is converted into a distorted trigonal bipyramidal shape, by a substitution in the Ge coordination sphere, which generated a set of shorter, parallel contacts visible in the projection of Figs. 9(b) and 9(c) leading to β-tin.

The competition between denser motifs characterizes therefore this metadynamics *megabasin* (1580–3260 metasteps). Importantly, motifs present at higher pressure, such as Ge(tI4), are still operating here, albeit not as lock-in

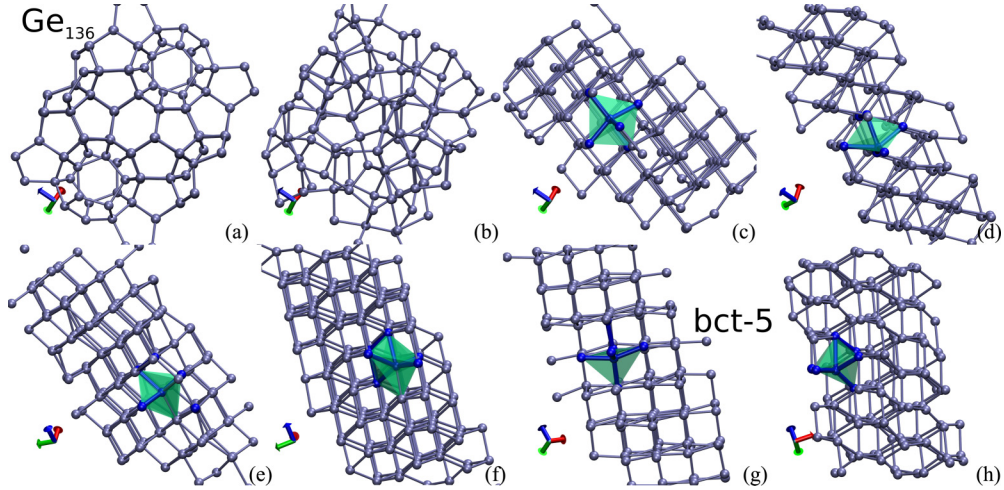

FIG. 8. (a)–(h) Snapshots from a metadynamics trajectory at $p = 2.5$ GPa and $T = 77$ K. The corresponding time steps are indicated in Fig. 7 as thick marks on the horizontal axis in the main panel. Ge_{136} (a) transforms into bct-5 (g) over several intermediates [(b)–(f)]. The region of stability of Ge_{136} (a) is followed by a region of substantially amorphous motifs of intermediate enthalpy values (b), which in turn evolves into a regime of lower enthalpy on average [(c)–(h)]. The latter is characterized by the occurrence of local fivefold coordination. Therein, β-tin is occasionally visited but fails to lock in at any point.

phases, but as transient motifs, particularly around bct-5, to which it can be mechanistically related in this low-pressure, low-temperature regime.

Based on our detailed mechanistic analysis, and previous results on the role of amorphization [38] at higher pressure, a synthetic pathway for bct-5 would therefore require separate steps, including (i) the amorphization of the clathrate motif at high pressure followed by (ii) recrystallization at a lower pressure such as 2.5 GPa. A possible way to accomplish this protocol might be a short shock wave, which would destabilize the clathrate framework, followed by a low-pressure regime, allowing the system to recrystallize. Alternatively, the application of anisotropic stress to the clathrate could induce both the amorphization at lower pressure and the crystallization to bct-5.

IV. CONCLUSIONS

The compression of Ge_{136} [Ge(cF136)] was studied by means of *ab initio* small-cell metadynamics. The choice of this approach, which makes no assumption regarding the final state, was meant to investigate the feasibility of recrystallization of the elusive bct-5 phase from specific precursors and to study under what conditions this pathway could be preferred. At $p = 5.0$ GPa and $T = 300$ K, the preferential product was identified as β-tin [Ge(tI4)]. At lower pressure ($p = 2.5$ GPa and $T = 300$ K), the fivefold-coordinated bct-5 appeared following pronouncedly anisotropic cell fluctuation. To shed further light on the competition between these two structural motifs, metadynamics runs were also performed at lower temperature, $T = 77$ K. β-tin remained accessible through direct compression at higher pressures, while bct-5 appeared exclusively at lower pressure values. Additionally, lower-temperature metadynamics discloses a rich landscape of different, transient fivefold-coordinated structural motifs, which can in principle crystallize from amorphous precursors, generated by direct compression of Ge_{136}. Unlike β-tin, bct-5 does not contain any fivefold rings (see Fig. 8), which correlates with its vibrational entropy [45], and has a comparatively higher enthalpy per atom. The combination of low pressure, low temperature, nonhydrostatic compression, and sufficient time to allow for crystallization can therefore be explored as a gateway for the synthesis of this elusive phase, while higher pressures appear to consistently favor β-tin [Ge(tI4)] [38] due to fast crystallization kinetics.

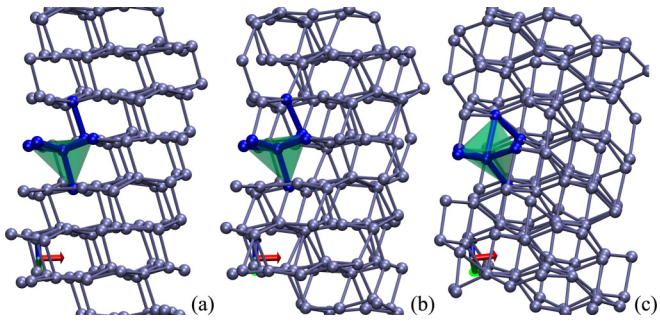

FIG. 9. (a)–(c) Three snapshots from the final part of the metatrajectory of Figs. 7 and 8: bct-5 transforms into a five-membered connected structural motif via a substitution mechanism in the Ge first coordination sphere. The structural motif of Ge(tI4) is visible in (c). The projection was chosen to emphasize the shortening of Ge-Ge contacts caused by this process.

V. METHODS

A. Metadynamics

Metadynamics [31–34] allows for the exploration of the energy surface along one or more collective reaction coordinates. The method is independent of the level of theory used, it does not require prior knowledge of the energy landscape, and its sampling efficiency can be enhanced by parallel runs started from different configurations. The time evolution of the system is biased by a history-dependent potential, which discourages the system from visiting already harvested

regions of the potential [46]. Efficiency is achieved in metadynamics also through dimensionality reduction. Instead of studying the problem in the full $3N$-dimensional configuration space of N particles, a relatively small number of collective coordinates $\mathbf{s} = (s_1 \cdots s_m)$ are used instead, which provide a coarse-grained description of the system and are able to distinguish between different free-energy minima, i.e., different phases. The inclusion of slow degrees of freedom in the space of collective variables positively impacts the performance of the method.

Each metadynamics metastep consisted of a molecular dynamics run in the NVT ensemble for a total simulation time of 0.5 ps (time step 2 fs) at either 300 K or at liquid nitrogen temperature, 77 K, depending on the regime studied. All metadynamics runs were performed with 34 atoms in the simulation box, which served as a collective (six-dimensional) variable. The size of the minimal box ensured commensurability of all already known phases, either open or dense, including Ge(cF136).

B. Density functional computational layers

SIESTA [37] was used as the density functional theory (DFT) molecular dynamics layer. For all compression protocols, electronic states were expanded by a single-ζ basis set constituted of numerical orbitals with a norm-conserving Troullier-Martins pseudopotential description of the core electrons [47]. The single-ζ basis set dramatically reduces computational times providing, nonetheless, the right topology and energy differences of all the Ge allotropes under study. The charge density was represented on a real-space grid with an energy cutoff [37] of 200 Ry. A Monkhorst-Pack k-point mesh of $2 \times 2 \times 2$ ensured the convergence of the electronic part.

C. Structure characterization

To accurately trace the structure evolution in the metadynamics simulations, the average size of the shortest circuits in the structures was calculated [48]. The average circuit size for Ge(cF136) is 5.12, while for β-tin it is 4.67. The average circuit size should decrease along the transition from the clathrate phase to the β-tin phase due to a reduction in the number of fivefold rings.

To discriminate between β-tin and bct-5 networks, coordination sequences (CSs, up to the third shell) were calculated at each metastep. For β-tin the CS reads (one atom type) as follows: 6, 22, 46. For bct-5 it is (one atom type) 5, 16, 33. Coordination sequences were also used to estimate the percentage of a phase (either β-tin or bct-5) along a metadynamics run, by looking for atoms with either $CS_{\text{bct-5}}$ 5, 16, 33 or $CS_{\beta\text{-tin}}$ 6, 22, 46.

In the case of new structures, ideal space group and asymmetric units were identified with the Generation, Analysis and Visualization of Reticular Ornaments using GAVROG Symmetry, Structure (Recognition) and Refinement (GAVROG SYSTRE) package [49].

ACKNOWLEDGMENTS

R.M. was supported by the Slovak Research and Development Agency under Contract No. APVV-19-0371 and by VEGA Project No. 1/0640/20. S.L. thanks the DFG for support under Priority Project No. SPP 1415 and under a personal Heisenberg fellowship, as well ARCCA Cardiff for the generous allocation of computational resources. S.L. also thanks the Leverhulme Trust for support under Project No. RPG-2020-052. Via our membership in the UK's HPC Materials Chemistry Consortium, which is funded by EPSRC (Grant No. EP/L000202), this work made use of the facilities of ARCHER, the UK's National High-Performance Computing Service, which is funded by the Office of Science and Technology through EPSRC's High End Computing program. This work also used the Isambard 2 UK National Tier-2 HPC Service [50] operated by GW4 and the UK Meteorological Office and funded by EPSRC (Grants No. EP/T022078/1 and No. EP/W03218X/1). We thank Nick Rivier for discussions.

[1] A. Mujica, A. Rubio, A. Munoz, and R. Needs, Rev. Mod. Phys. **75**, 863 (2003).
[2] H. B. Cui, D. Graf, J. S. Brooks, and H. Kobayashi, Phys. Rev. Lett. **102**, 237001 (2009).
[3] X.-J. Chen, C. Zhang, Y. Meng, R.-Q. Zhang, H.-Q. Lin, V. V. Struzhkin, and H.-k. Mao, Phys. Rev. Lett. **106**, 135502 (2011).
[4] U. Schwarz, Z. Kristallogr. **219**, 376 (2004).
[5] H. Katzke and P. Tolédano, J. Phys.: Condens. Matter **19**, 275204 (2007).
[6] A. Mujica, C. J. Pickard, and R. J. Needs, Phys. Rev. B **91**, 214104 (2015).
[7] C. Claeys, J. Mitard, G. Eneman, M. Meuris, and E. Simon, in *Proceedings of the EMRS 2009 Spring Meeting Symposium I: Silicon and Germanium Issues for Future CMOS Devices*, Thin Solid Films Vol. 518 (IMEC, Louvain, Belgium, 2010), pp. 2301–2306.
[8] D. Li, Y. Ma, and J. Yan, Phys. Rev. Lett. **104**, 139701 (2010).
[9] H. B. Cui, D. Graf, J. S. Brooks, and H. Kobayashi, Phys. Rev. Lett. **104**, 139702 (2010).
[10] S. Lewis and M. Cohen, Solid State Commun. **89**, 483 (1994).
[11] C. S. Menoni, J. Z. Hu, and I. L. Spain, Phys. Rev. B **34**, 362 (1986).
[12] R. J. Nelmes, H. Liu, S. A. Belmonte, J. S. Loveday, M. I. McMahon, D. R. Allan, D. Häusermann, and M. Hanfland, Phys. Rev. B **53**, R2907 (1996).
[13] Y. K. Vohra, K. E. Brister, S. Desgreniers, A. L. Ruoff, K. J. Chang, and M. L. Cohen, Phys. Rev. Lett. **56**, 1944 (1986).
[14] K. Takemura, U. Schwarz, K. Syassen, M. Hanfland, N. E. Christensen, D. L. Novikov, and I. Loa, Phys. Rev. B **62**, R10603 (2000).
[15] V. V. Brazhkin, A. G. Lyapin, S. V. Popova, and R. N. Voloshin, Phys. Rev. B **51**, 7549 (1995).
[16] B. Haberl, M. Guthrie, B. D. Malone, J. S. Smith, S. V. Sinogeikin, M. L. Cohen, J. S. Williams, G. Shen, and J. E. Bradby, Phys. Rev. B **89**, 144111 (2014).
[17] U. Schwarz, A. Wosylus, B. Böhme, M. Baitinger, M. Hanfland, and Y. Grin, Angew. Chem. Int. Ed. **47**, 6790 (2008).

[18] A. Wosylus, Y. Prots, W. Schnelle, M. Hanfland, and U. Schwarz, Z. Naturforsch. B: J. Chem. Sci. **63**, 608 (2008).
[19] C. Cros, M. Pouchard, and P. Hagenmuller, J. Solid State Chem. **2**, 570 (1970).
[20] J. S. Kasper, P. Hagenmuller, M. Pouchard, and C. Cros, Science **150**, 1713 (1965).
[21] A. San-Miguel, P. Kéghélian, X. Blase, P. Melinon, A. Perez, J. P. Itié, A. Polian, E. Reny, C. Cros, and M. Pouchard, Phys. Rev. Lett. **83**, 5290 (1999).
[22] P. Melinon, P. Kéghélian, X. Blase, J. Le Brusc, A. Perez, E. Reny, C. Cros, and M. Pouchard, Phys. Rev. B **58**, 12590 (1998).
[23] A. A. Demkov, W. Windl, and O. F. Sankey, Phys. Rev. B **53**, 11288 (1996).
[24] S. Saito and A. Oshiyama, Phys. Rev. B **51**, 2628 (1995).
[25] R. Nesper, K. Vogel, and P. E. Blöchl, Angew. Chem. Int. Ed. Engl. **32**, 701 (1993).
[26] M. O'Keeffe, G. B. Adams, and O. F. Sankey, Phys. Rev. Lett. **68**, 2325 (1992).
[27] A. M. Guloy, R. Ramlau, Z. Tang, W. Schnelle, M. Baitinger, and Y. Grin, Nature (London) **443**, 320 (2006).
[28] R. J. Nelmes, M. I McMahon, N. G. Wright, D. R. Allan, and J. S. Loveday, Phys. Rev. B **48**, 9883 (1993).
[29] C. H. Bates, F. Dachille, and R. Roy, Science **147**, 860 (1965).
[30] F. P. Bundy and J. S. Kasper, Science **139**, 340 (1963).
[31] A. Laio and M. Parrinello, Proc. Natl. Acad. Sci. USA **99**, 12562 (2002).
[32] R. Martoňák, A. Laio, and M. Parrinello, Phys. Rev. Lett. **90**, 075503 (2003).
[33] R. Martoňák, D. Donadio, A. R. Oganov, and M. Parrinello, Nat. Mater. **5**, 623 (2006).
[34] R. Martoňák, Eur. Phys. J. B **79**, 241 (2011).
[35] D. Selli, I. A. Baburin, R. Martoňák, and S. Leoni, Sci. Rep. **3**, 1466 (2013).
[36] M. W. Guinan and D. J. Steinberg, J. Phys. Chem. Solids **35**, 1501 (1974).
[37] J. Soler, E. Artacho, J. Gale, A. Garcia, J. Junquera, P. Ordejón, and D. Sánchez-Portal, J. Phys.: Condens. Matter **14**, 2745 (2002).
[38] M. Ryník, S. Leoni, and R. Martoňák, Phys. Rev. B **105**, 134107 (2022).
[39] V. L. Deringer, N. Bernstein, G. Csányi, C. Ben Mahmoud, M. Ceriotti, M. Wilson, D. A. Drabold, and S. R. Elliott, Nature (London) **589**, 59 (2021).
[40] V. Buch, R. Martoňák, and M. Parrinello, J. Chem. Phys. **123**, 051108 (2005).
[41] Herein, we use the term "shortest circuits" to emphasize that they are in general different from rings, which are often used to characterize the local structure of amorphous materials. In short, rings are circuits with the special property that any circuit can be written as a disjunctive sum of rings, i.e., rings form a basis for the cycle space of a graph.
[42] S. T. Hyde and S. J. Ramsden, in *Chemical Topology: Applications and Techniques*, edited by D. Bonchev and D. H. Rouvray Mathematical Chemistry Series Vol. 6, (Gordon and Breach, New York, 1999), pp. 35–174.
[43] N. Rivier and F. Wooten, MATCH **48**, 145 (2003).
[44] F. Wooten, Acta Crystallogr. Sect. A: Found. Crystallogr. **58**, 346 (2002).
[45] J. Friedel, J. Phys. Lett. **35**, 59 (1974).
[46] A. Laio and F. L. Gervasio, Rep. Prog. Phys. **71**, 126601 (2008).
[47] N. Troullier and J. L. Martins, Phys. Rev. B **43**, 1993 (1991).
[48] V. Blatov, in *IUCr CompComm Newsletter No. 7* (IUCr Commission on Crystallographic Computing, Berkeley, CA, 2006), p. 4, https://www.iucr.org/resources/commissions/computing/newsletters/7.
[49] O. Delgado-Friedrichs, http://gavrog.org/, 2006.
[50] http://gw4.ac.uk/isambard/.